

BALLISTIC IMPACTS AGAINST THIN METALLIC ALUMINIUM 1100-H12 TARGET PLATE: A VALIDATION STUDY OF NUMERICAL SIMULATION USING LS-DYNA

Syazana Auni Mohd Hushin^a, Mohd Zaid Othman^{a*}, Jestin Jelani^b, Tan Kean Sheng^a, Khairul Hasni Kamarudin^a, Amir Radzi Ab Ghani^c

^a Department of Mechanical Engineering, Faculty of Engineering, National Defence University of Malaysia, Sungai Besi Camp, 57000 Kuala Lumpur, Malaysia

^b Department of Civil Engineering, Faculty of Engineering, National Defence University of Malaysia, Sungai Besi Camp, 57000 Kuala Lumpur, Malaysia

^c College of Engineering, MARA University of Technology (UiTM), 40450 Shah Alam, Selangor, Malaysia

ARTICLE INFO

ARTICLE HISTORY

Received: 12-07-2023

Revised: 01-09-2023

Accepted: 10-11-2023

Published: 31-12-2023

KEYWORDS

Ballistic

Impact

LS-DYNA

Numerical simulation

Projectile

ABSTRACT

In this study, eight sets of numerical simulation analyses by using LS-DYNA were performed to predict the performances of four different types of projectiles head impacted against single and double circular target plates. The projectiles were impacted in three angles of incidence i.e. 0, 15 and 30 degrees relative to the positive horizontal x-axis. To validate the simulations, experimental tests result from a published paper was utilized, where the residual velocities of the projectile after it penetrated the plate, and the deformation patterns failures of the target plate were duly compared. In general, the numerical simulations analyses for all eight sets of tests had managed to produce good agreement with respect to the experimental tests data from a published paper with an overall average percentage difference residual velocity of 16.14 % in predicting the residual velocities of the projectiles upon exiting the target plate.

1.0 INTRODUCTION

Ballistic research in the areas of military applications, protective structures, aerospace structures are vast and well documented in the open literatures [1-7]. Past studies in the areas of ballistics impact include the different head of projectiles shapes, fracture criterion, ballistic resistance, various target plate thicknesses, target plate boundary conditions, projectile velocities, parameters of the projectiles, ballistic designs, effects of inclined angles, slenderness ratios, soft tissue damage, wound ballistic, protection gear design, penetration dynamics, projectile density and projectile diameter [8-14]. Previous investigations also showed that plug and petal types of failures were closely connected with ballistic impact various nose geometries of projectiles against thin ductile targets [15]. When a projectile hits a thin ductile target plate, among the critical factors that affect the successful failure of the target plate are the impact angle; ie defined as the angle that is situated between the projectile longitudinal axis and the perpendicular surface of the target plate, the actual physical condition where the target plate is fixed rigidly, the three dimensional nose shape of the projectile and the type of substances by which the projectile and target plate are made from [16].

The main objective of this present study is to create realistic simulation model by validating against experimental test data of the ballistic impact phenomena of four different types of projectiles onto aluminium 1100-H12 circular target plate [16]. Four different types of projectiles nose geometries will be modelled, each of the projectiles will be given their respective velocities and will impact the circular target plate at variable angles and finally the residual velocities as predicted by the numerical simulations will be validated against the experimental results obtained from the published work [16].

*Corresponding Author | Othman, M. Z. | zaid002@gmail.com

2.0 NUMERICAL SIMULATION METHODOLOGY

Experimental tests results from a published research paper [16] will be utilized to validate and measure the accuracy of the numerical simulations predictions produced in this study. Three dimensional numerical simulation studies were performed by utilizing LS-PREPOST and LS-DYNA to simulate the experimental tests as reported in a published paper [16] i.e. all of the four different types of projectiles impacted onto a circular plate target rigidly fixed around its circumferential perimeter (see Figure 1 and Figure 2). The geometric modelling of the projectiles, the circular target plates, material assignments, boundary conditions, velocity assignments and contact assignments were performed by using the relevant keywords in LS-PREPOST while the completed numerical simulations programs were processed by using LS-DYNA.

All of the projectiles were made from rigid type EN-24 steel bar and had the same mass and the circular target plate was made from deformable type aluminium 1100-H12 [16]. Figure 2 shows the general arrangements of the projectile and the circular target plate, whereby the projectile was located to the left of the circular target plate with the target plate positioned in a perpendicular direction with respect to the projectile. After the projectile had been assigned with the respective velocity, it will travel to the right direction and will impact the central portion of the circular target plate. Among the variables of the impact phenomenon of the projectile against the target plate that were modelled in the numerical simulation studies include the different geometry shape of the projectiles, the angle of impact, velocity of impact and the number of target plate.



Figure 1. The circular target plate fully fixed around its outer perimeter leaving a 255 mm in diameter central exposed area [16]

Table 1 shows the complete list of a total number of eight numerical simulation analyses that were performed in this validation study. Briefly, it could be observed that there were four main pairs of tests that were utilized in the numerical simulation studies with only slight differences in the numerical and alphabetical wordings as observed in the Test number. For example, the numerical number '1' as shown in 'Test 1A' represents the type of projectile used in the numerical simulation study i.e. ogive nosed (see Figure 3); while '2', '3' and '4' refers to the blunt, conical and hemispherical nosed shaped projectiles, respectively (see Figure 4, Figure 5, Figure 6). Located next to the right side of the numerical number, the alphabet 'A' refers to a single target plate of 2 mm in total thickness while the alphabet 'B' refers to a double target plate of 2 unit's x 1 mm, which would still give a total of 2 mm of thickness for the target plate. All of these eight tests involved the projectile impacting the circular target plate at 0 degree, 15 degrees and 30 degrees with respect to the horizontal x-axis (see Figure 2).

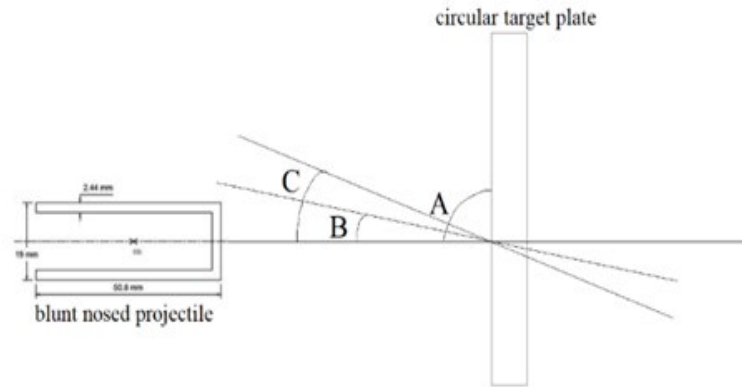


Figure 2. The angle of incidences where the projectile impacts the circular target plate (A=90 degrees, B=15 degrees and C=30 degrees)

Table 1. The respective test numbers for the four different types of projectiles impacted against the target plates as modelled in the numerical simulation studies

Test number	Description
Test 1A	Ogive nosed projectile impacted against 1 unit x 2 mm thickness of circular target plate (single layered)
Test 1B	Ogive nosed projectile impacted against 2 units x 1 mm thickness of circular target plate (double layered)
Test 2A	Blunt nosed projectile impacted against 1 unit x 2 mm thickness of circular target plate (single layered)
Test 2B	Blunt nosed projectile impacted against 2 units x 1 mm thickness of circular target plate (double layered)
Test 3A	Conical nosed projectile impacted against 1 unit x 2 mm thickness of circular target plate (single layered)
Test 3B	Conical nosed projectile impacted against 2 units x 1 mm thickness of circular target plate (double layered)
Test 4A	Hemispherical nosed projectile impacted against 1 unit x 2 mm thickness of circular target plate (single layered)
Test 4B	Hemispherical nosed projectile impacted against 2 units x 1 mm thickness of circular target plate (double layered)

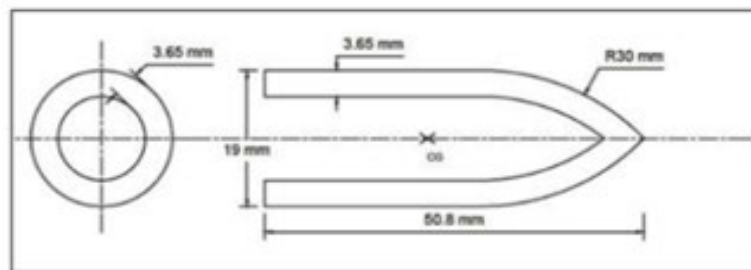


Figure 3. The cross-sectional dimensions for an ogive nosed projectile for Tests 1A and 1B [16]

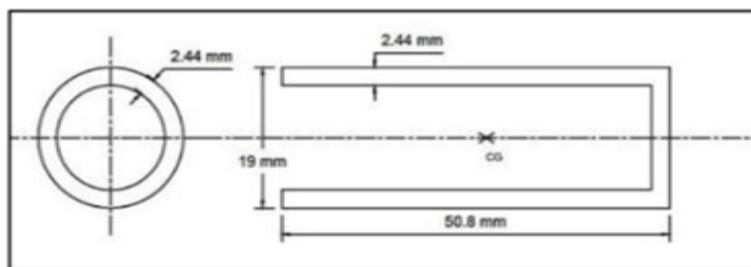


Figure 4. The cross-sectional dimensions for a blunt nosed projectile for Tests 2A and 2B [16]

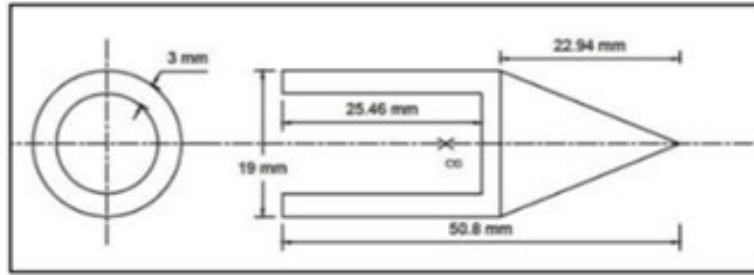


Figure 5. The cross-sectional dimensions for a conical nosed projectile for Tests 3A and 3B [16]

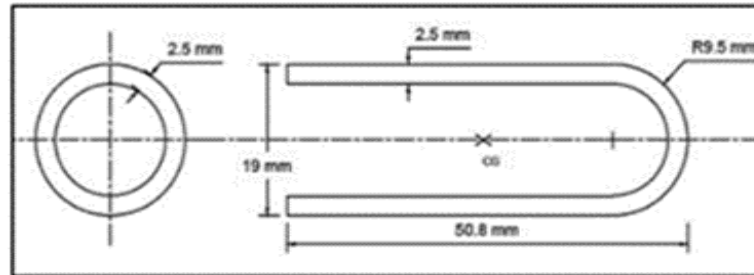


Figure 6. The cross-sectional dimensions for a hemispherical nosed projectile for Tests 4A and 4B [16]

Figure 7 shows the three-dimensional conical nosed shape projectile modelled by using 8,136 rigid elements, while Figure 8 shows the three-dimensional circular target plate modelled by using 15,125 deformable elements in LS-PREPOST. The projectile was constructed by using rigid elements, where it was assumed that the projectile will not undergo any kind of deformations i.e. *MAT_020_RIGID keyword and its material properties are as shown in Table 2. The circular target plate was made from aluminium 1100-H12 with its assigned Johnson-Cook material properties i.e. *MAT_015_JOHNSON_COOK keyword together with its corresponding equation of state (EOS) i.e. *EOS keyword (see Table 3 and Table 4). Figure 1 and Figure 2 show the experimental test arrangements of the projectile that moved to the right with the assigned velocity impacting the circular target plate that was fully constrained around its perimeter; rigidly held in its vertical position by a combination of two pieces of circular rings, bolts, and nuts. To simulate these scenarios, boundary conditions keywords will be utilized in the numerical simulation analysis to replicate the event. The projectile will be fully constrained to move in all directions except to the right i.e. x-direction with an assigned amount of velocity i.e. *INITIAL_VELOCITY_GENERATION keyword. Figure 9 shows the circular target plate three-dimensional model where the nodes on its circumference and the nodes that were located along its thickness were fully fixed in all directions i.e. *BOUNDARY_SPC_SET_ID keyword was utilized to replicate that it was rigidly held as observed in the experimental test arrangements. *AUTOMATIC_SURFACE_TO_SURFACE keyword was employed in the program to create the contact interactions between the projectile (assigned as slave part) and the circular target plate (assigned as master part). Once the relevant keywords had been fully utilized in constructing the numerical simulation analysis, the program was then sent to LS-DYNA for processing and the results are presented in the next section.

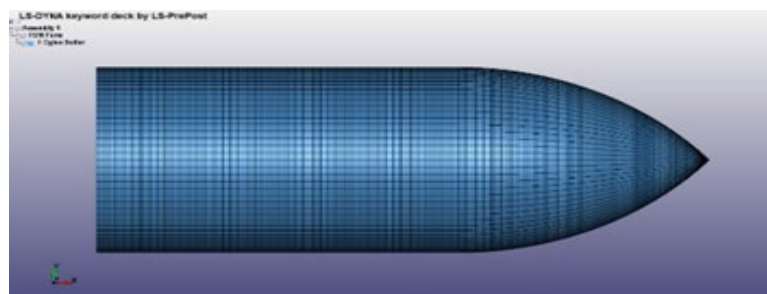


Figure 7. Three-dimensional ogive nosed shape projectile modelled in LS-PREPOST

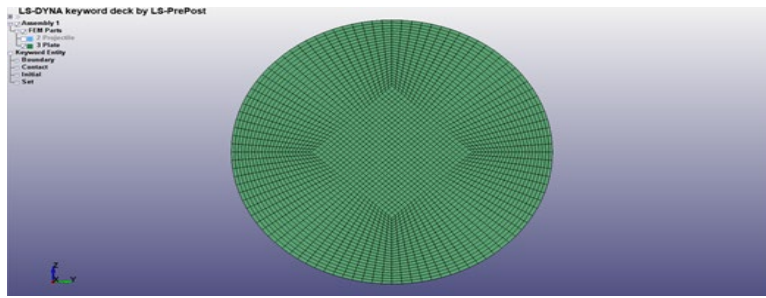


Figure 8. Three-dimensional circular plate target modelled in LS-PREPOST

Table 2. The material properties for the rigid projectile [16]

Material Properties	Value
Mass Density, ρ (kg/m ³)	7650
Young modulus, E (GPa)	100
Poisson's ratio, ν	0.3

Table 3. Johnson-Cook's material properties for the target plate i.e. aluminium 1100-H12 [16]

Material Properties	Value
Young modulus of elasticity, E (GPa)	65.76
Poisson's ratio, ν	0.3
Proof/Yield stress, A (MPa)	102.75
Strain hardening coefficient, B (MPa)	168.11
Strain hardening exponent, n	0.1012
Strain sensitivity coefficient, C	0.001
Thermal softening constant, m	0.859

Table 4. Gruneisen EOS parameters for the circular target plate i.e. aluminium 1100-H12 [17]

Parameters	Value
C (m/s)	5240
S_1	1.4
S_2	0.0
S_3	0.0
Γ	1.97
A	0.48

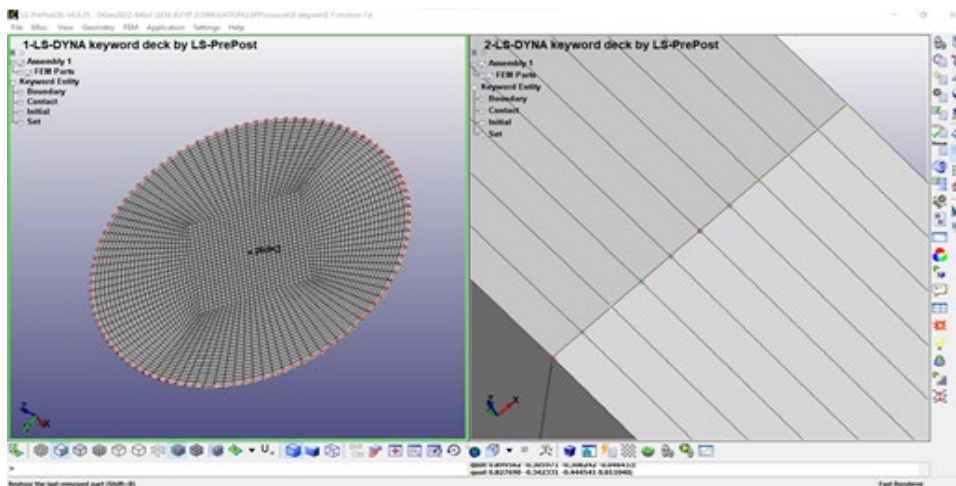


Figure 9. The boundary conditions of the circular target plate where it was fully constrained around its circumference

3.0 RESULTS AND DISCUSSION

All the eight numerical simulation analyses tests results of the four different types of projectiles impacted against the circular target plate processed by LS-DYNA (see Table 1) are presented in this section. In

general, the LS-DYNA validations results i.e. residual velocities and deformation patterns obtained in this study are presented and compared with the data of the residual velocities obtained from the experimental tests and numerical simulations analyses i.e. ABAQUS of the published paper [16]. Each of the numerical simulations tests results e.g. for Test 1A, is presented in pairs on one complete A4 page with a total of eight A4 pages to accommodate all of the eight tests results (see Table 1). For example, the LS-DYNA results for Test 1A i.e. ogive nosed projectile impacted against 1 unit of 2 mm in thickness of the circular target plate are presented in two parts (see Table 5 and Figure 10). The first part consists of a table of data that compares the LS-DYNA results against the ABAQUS and experimental test data [16] for three different angles at different velocities and the second part shows selected LS-DYNA deformations patterns of the circular target plate for three different angles against the deformations patterns obtained by ABAQUS and the experimental test data [16].

Residual velocities' results for Test 1A i.e. ogive nosed projectile impacted against single circular plate showed that the overall average percentage for all three angles of impact to be around 24.23 % (see Table 5) which are acceptable values and it could be observed that the deformations patterns for all three angles of impact as produced by LS-DYNA (see Figure 10) closely resembled the deformations patterns obtained from the actual experimental tests [16]. A very good agreement for both of the overall average percentage for all three angles of impact against double circular target plate of 4.8 % (see Table 6) and the deformations patterns as predicted by LS-DYNA (see Figure 11) can be observed for Test 1B results.

Total average residual velocities' percentage differences of 19.4 % can be noticed for the impact of blunt nosed projectile against single circular target plate for Test 2A residual velocities' results (see Table 7). The deformation patterns as predicted by LS-DYNA for Test 2A were in very good agreement with the failure patterns of the single target plate obtained from the experimental tests data (see Figure 12). A circular shaped failure pattern, an almost ellipse petal like failure pattern and an oblong petal like failure pattern can be recognized for 0, 15 and 30 degrees of angle of projectile impact, respectively (see Figure 12). A better total average percentage differences of 6 % can be seen for the LS-DYNA residual velocities predictions for Test 2B against the experimental tests data for the impact of blunt nosed projectile against double layered circular plate (see Table 8). The deformation patterns as predicted by LS-DYNA too were very good in agreement with the experimental tests data where a circular shape failure pattern followed by both oblong shape failure patterns could be observed for 0, 15 and 30 degrees of angle of projectile impact, respectively (see Figure 13).

Table 9 shows an absolute average residual velocity percentage difference of 10 % produced by LS-DYNA for Test 3A i.e. conical nosed projectile impacted against single circular target plate (see Table 9). Figure 14 shows the deformation patterns for all of the three angles of impact (0, 15 and 30 degrees) as predicted by LS-DYNA that were in good agreement with the experimental tests data and closely resembled circular failure configurations that can be seen in the physical experimental tests results for the single circular target plate (see Figure 14). Table 10 shows an overall average residual velocity percentage difference of 13 % predicted by LS-DYNA for Test 3B i.e. conical nosed projectile impact against double layered target plate. Figure 15 displays the deformation patterns of the double layered plate, where good agreement of almost circular shape failure mode was predicted by LS-DYNA that was like the result from the experimental test specifically for 0-degree angle. Unfortunately, LS-DYNA predictions did not manage to give good predictions for 15-degree and 30-degrees angles for Test 3B, where it predicted an almost circular shape failure mode as opposed to an oblong shape failure mode as were observed in the experimental tests results.

Table 11 presents the overall average residual velocity percentage differences of 22 % produced by LS-DYNA for Test 4A i.e. hemispherical nosed projectile impacted against single circular target plate (see Table 11). Figure 16 displays the deformation patterns of the double layered circular target plate produced by LS-DYNA, where it could be seen that for both of the 0 and 15 degrees of angle of projectile; LS-DYNA had successfully predicted an almost circular shape type of failure but for the 30 degree of angle of projectile; LS-DYNA predicted an almost circular shape type of failure whereas an oblong petal like failure mode was observed in the experimental test data. Table 12 describes the comprehensive average residual velocity percentage differences of 26 % produced by LS-DYNA for Test 4B i.e. hemispherical nosed projectile impacted against double layered circular target plate. Figure 17 displays Test 4B tests results i.e. the deformation patterns of circular shape like failure modes for all three angles of projectiles i.e. 0, 15 and 30 degrees, produced by LS-DYNA which was in good agreement for 0 degree angle of

projectile only but differed for the 15 and 30 degrees of angle of projectiles as shown in the experimental tests data where both of these angle of projectiles experienced petal oblong shape like failure mode.

Some of the contributing factors that might influenced the large values of average residual velocity percentage differences are discussed in this section. The exact values of coefficient of friction between the projectile and circular target plate, specific heat, mass density, shear modulus and Gruneisen equation of state parameters for aluminium 1100-H12 were not available from the published paper [16], thus these values had to be obtained from the open literature and these may have significant effects on the accuracy of the results. In the actual experimental test, originally the circular target plate had a diameter greater than 255 mm. To rigidly hold the circular target plate in its vertical position, the outer circular target plate's circumference was clamped by two steel rings of 30 mm in width with 8 equally spaced bolts around its circumference leaving an exposed circular surface of 255 mm in diameter (see Figure 1). In the numerical simulation, to simplify the geometry and boundary conditions of the circular target plate, only a circular plate of 255 mm in diameter was modelled. Its outer perimeter was fully fixed in the translational x, y, and z directions so that it is rigidly fixed in the vertical position like its conditions in the physical experimental scenario. These differences in the way the circular target plate's geometry and the way the setting up of the boundary conditions of the circular target plate in the numerical simulation may have contributed to the discrepancies in the outcome of the predictions. The exact location where the values of the initial velocity and the residual velocity of the projectile were not clearly defined in the performed experimental tests [16], whereas in the numerical simulation analysis, the assigned initial velocity of the projectile was located just before it hits the circular target plate and the residual velocity of the projectile was taken just after it exited the circular target plate. Thus, the variations in determining the exact location of the projectile in the experimental tests and numerical simulation may also influence the final predictions by LS-DYNA.

Table 5. LS-DYNA validation results for Test 1A, ogive nosed projectile impacted against 1 unit x 2 mm thickness of circular plate (single layered target plate) [16]

Angle	Initial Velocity (m/s)	Residual Velocity (m/s)			Percentage Difference (%)	Average Percentage Differences (%)
		ABAQUS	Experimental	LS-DYNA		
0°	107.7	78.2	83.4	70.8	16.3	22.1
	102.7	70.9	76.8	63.2	19.4	
	95.4	58.9	54.7	51.1	6.8	
	84.5	39.6	42.6	26.7	45.9	
15°	134.7	111.5	116.4	104.0	11.3	20.0
	124.5	98.8	108.5	89.2	19.5	
	113.5	84.2	94.2	74.5	23.4	
	92.3	50.5	57.4	74.5	25.9	
30°	122.0	92.2	98.7	81.2	19.5	30.6
	113.8	80.3	85.6	68.2	22.6	
	105.5	67.1	72.9	52.6	32.4	
	93.1	44.8	51.6	31.7	47.8	

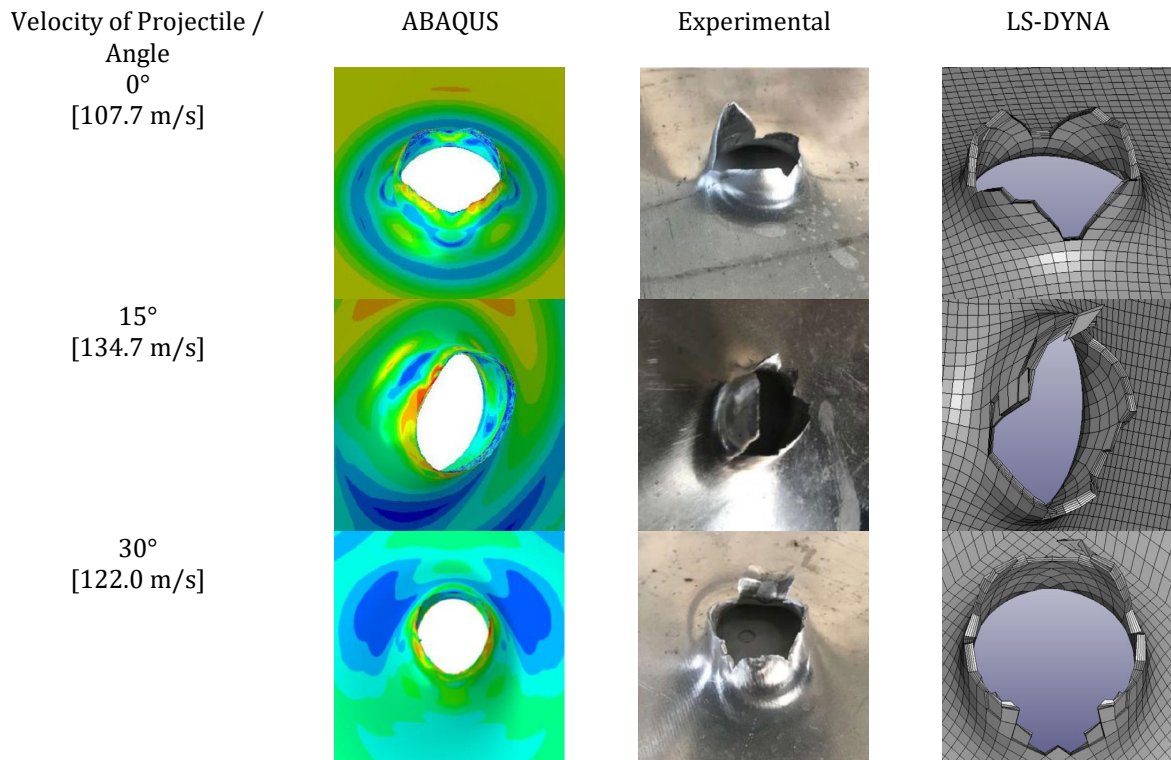


Figure 10. LS-DYNA deformation pattern results for Test 1A, ogive nosed projectile impacted against 1 unit x 2 mm thickness of circular target plate for the three different angles (single layered target plate) [16]

Table 6. LS-DYNA validation results for Test 1B, ogive nosed projectile impacted against 2 units x 1 mm thickness of circular target plate (double layered target plate) [16]

Angle	Initial Velocity (m/s)	Residual Velocity (m/s)			Percentage Difference (%)	Average Percentage Differences (%)
		ABAQUS	Experimental	LS-DYNA		
0°	112.5	88.4	89.7	87.3	2.7	4.4
	105.8	79.8	78.0	76.6	1.8	
	103.8	76.6	78.7	75.1	4.7	
15°	97.3	67.0	70.8	65.1	8.4	2.9
	113.9	89.6	90.5	89.0	1.7	
	108.7	82.7	84.7	82.6	2.5	
	101.9	73.5	76.8	71.8	6.7	
30°	82.3	36.5	42.3	42.6	0.7	7.1
	131.7	109.5	110.8	109.0	1.6	
	126.0	102.3	105.6	100.0	5.4	
	116.3	89.9	94.5	88.3	6.8	
	111.3	83.2	90.2	81.4	10.3	
	79.6	25.6	30.5	27.2	11.4	

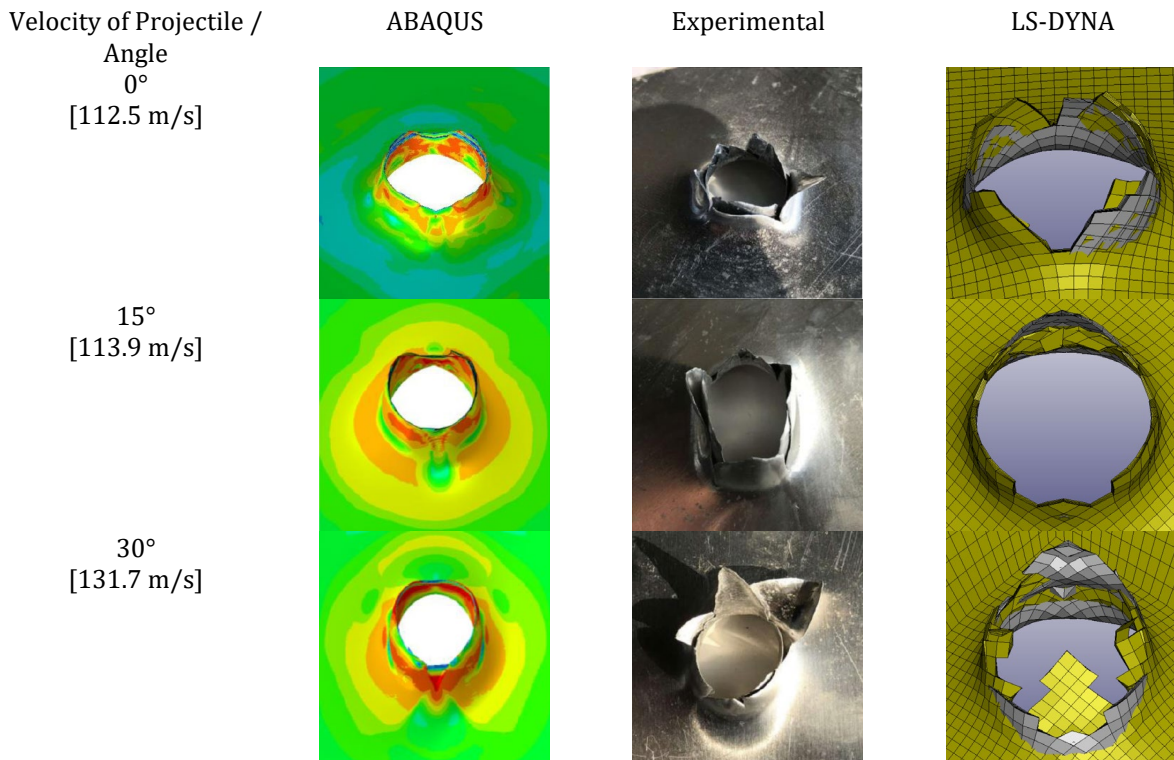


Figure 11. LS-DYNA deformation pattern results for Test 1B, ogive nosed projectile impacted against 2 units x 1 mm thickness of circular target plate (double layered target plate) [16]

Table 7. LS-DYNA validation results for Test 2A, blunt nosed projectile impacted against 1 unit x 2 mm thickness of circular target plate (single layered target plate) [16]

Angle	Initial Velocity (m/s)	Residual Velocity (m/s)			Percentage Difference (%)	Average Percentage Differences (%)
		ABAQUS	Experimental	LS-DYNA		
0°	120.2	90	92.5	77.1	18.2	22.1
	113.7	80.3	84.8	67.0	23.5	
	110.1	73.6	78.3	61.2	24.5	
15°	90.3	27.8	32.6	*	*	20.5
	106.0	66.8	69.6	64.5	7.6	
	103.3	62.9	65.1	61.2	6.2	
	95.6	51.9	59.2	48.4	20.1	
30°	85.1	25.3	29.6	18.1	48.2	15.7
	141.4	115.6	124.4	98.0	23.7	
	132.9	105.8	108.5	87.0	22.0	
	121.2	89.6	94.2	83.0	12.6	
	102.5	69.1	76.7	66.0	15.0	
	80.1	23.5	27.4	28.8	5.0	

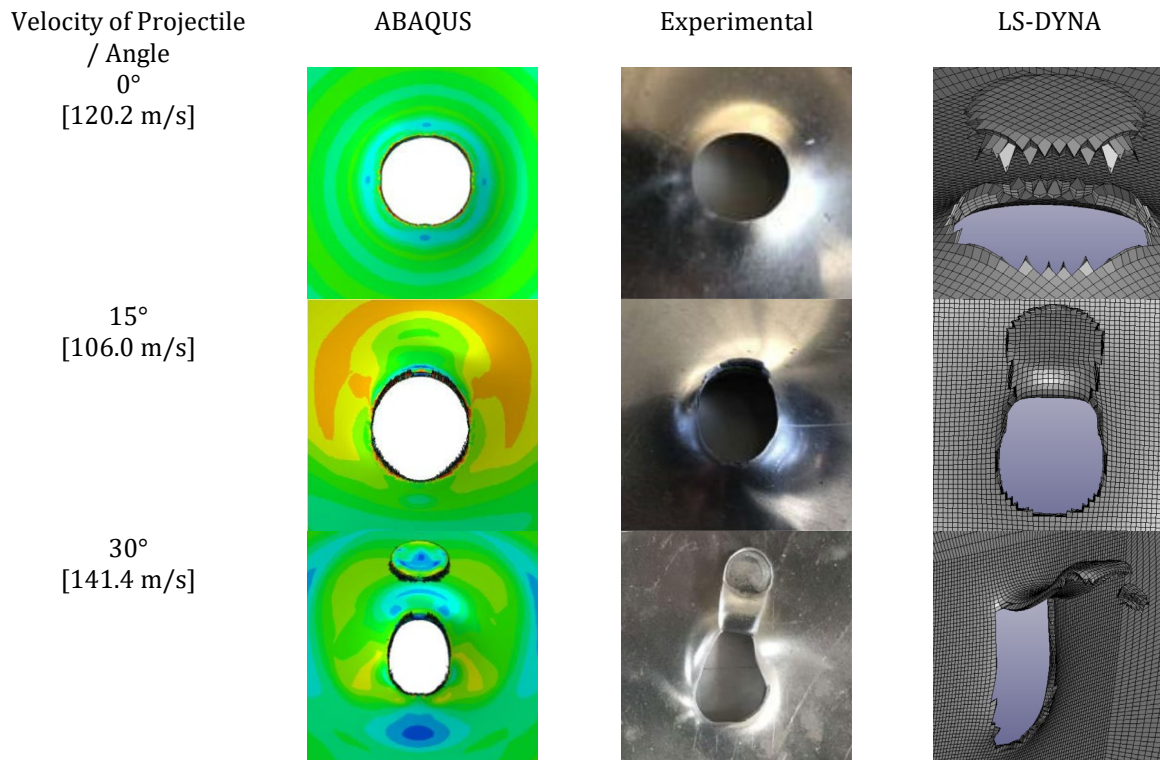


Figure 12. LS-DYNA deformation pattern results for Test 2A, blunt nosed projectile impacted against 1 unit x 2 mm thickness of circular target plate (single layered target plate) [16]

Table 8. LS-DYNA validation results for Test 2B, blunt nosed projectile impacted against 2 units x 1 mm thickness of circular target plate (double layered target plate) [16]

Angle	Initial Velocity (m/s)	Residual Velocity (m/s)			Percentage Difference (%)	Average Percentage Differences (%)
		ABAQUS	Experimental	LS-DYNA		
0°	126.9	92.6	101.2	115.0	12.8	8.3
	124.6	88.7	97.7	106.0	8.1	
	114.8	73.6	83.8	76.9	8.6	
	110.15	67.3	75.8	73.0	3.8	
	90.6	22.3	28.9	*	*	
15°	115.4	83.3	89.9	87.1	3.2	7.2
	109.6	75.1	82.6	80.1	3.1	
	103.7	65.7	72.7	71.5	1.7	
	101.1	60.5	65.5	67.1	2.4	
	90.2	34.5	39.6	51.3	25.7	
30°	119.2	87.6	94.5	94.1	0.4	5.24
	118.3	85.7	92.6	91.2	1.5	
	112.8	80.5	87.8	87.1	0.8	
	106.3	71.8	79.6	79.3	0.4	
	85.3	33.5	38.6	48.7	23.1	

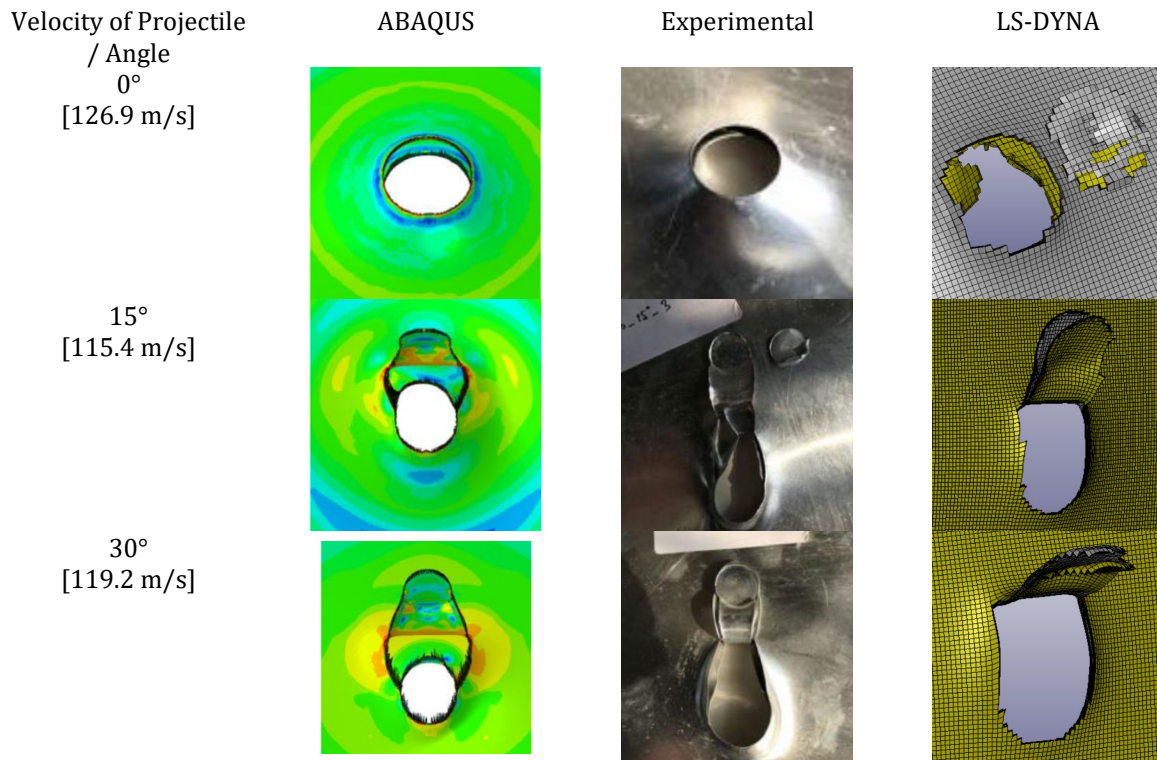


Figure 13. LS-DYNA deformation pattern results for Test 2B, blunt nosed projectile impacted against 2 units x 1 mm thickness of circular target plate (double layered target plate) [16]

Table 9. LS-DYNA validation results for Test 3A, conical nosed projectile impacted against 1 unit x 2 mm thickness of circular target plate (single layered target plate) [16]

Angle	Initial Velocity (m/s)	Residual Velocity (m/s)			Percentage Difference (%)	Average Percentage Differences (%)
		ABAQUS	Experimental	LS-DYNA		
0°	132.7	108.7	110.0	112.0	1.8	5.76
	116.3	87.9	90.4	94.3	4.2	
	113.9	84.4	87.3	91.3	4.5	
	108.7	77.2	83.4	84.4	1.2	
	85.3	35.9	41.3	49.0	17.1	
15°	129.1	102.2	111.1	108.0	2.8	13.36
	124.0	95.6	101.7	98.4	3.3	
	111.1	77.7	86.5	84.6	2.2	
	92.4	45.3	52.6	58.3	10.3	
	85.3	23.5	26.9	44.0	48.2	
30°	120.6	85.0	90.7	91.8	1.2	16.0
	116.1	78.2	85.2	92.9	8.6	
	108.3	65.0	70.8	70.8	0	
	102.1	52.6	57.8	63.8	9.9	
	90.1	19.3	23.5	43.9	60.5	

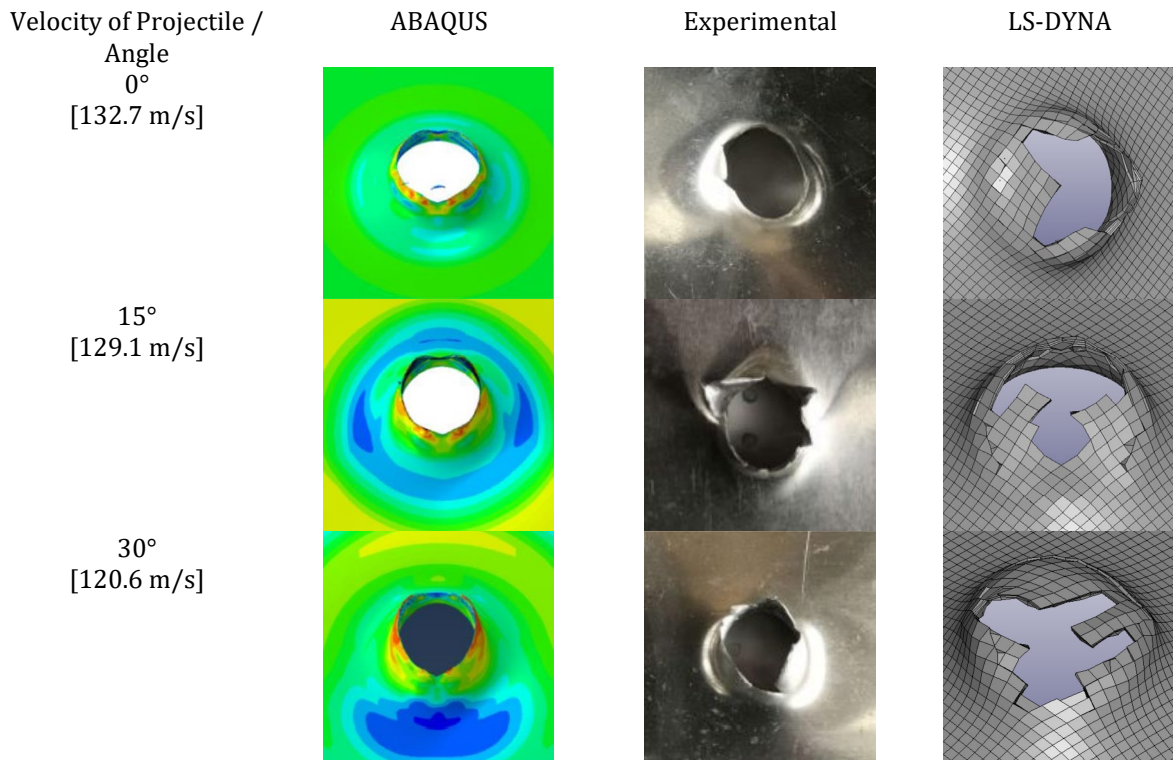


Figure 14. LS-DYNA deformation pattern results for Test 3A, conical nosed projectile impacted against 1 unit x 2 mm thickness of circular target plate (single layered target plate) [16]

Table 10. LS-DYNA validation results for Test 3B, conical nosed projectile impacted against 2 units x 1 mm thickness of circular target plate (double layered target plate) [16]

Angle	Initial Velocity (m/s)	Residual Velocity (m/s)			Percentage Difference (%)	Average Percentage Differences (%)
		ABAQUS	Experimental	LS-DYNA		
0°	116.5	91.8	95.7	98.6	2.9	14.9
	108.5	81.2	84.4	89.9	6.3	
	101.9	72.2	76.9	83.4	8.1	
	95.2	62.1	65.6	74.7	12.9	
	80.5	33.2	37.4	52.1	44.3	
15°	133.7	112.4	114.7	119.0	3.7	12.5
	123.3	99.7	100.9	108.0	6.8	
	92.3	57.0	61.3	70.2	13.5	
30°	85.6	42.7	47.6	61.9	26.1	13.8
	135.6	112.5	116.8	120.0	2.7	
	130.8	106.6	110.5	113.0	2.2	
	121.2	95.3	101.8	103.0	1.2	
	110.7	80.4	86.8	91.2	4.9	
	84.5	31.5	35.4	57.1	57.8	

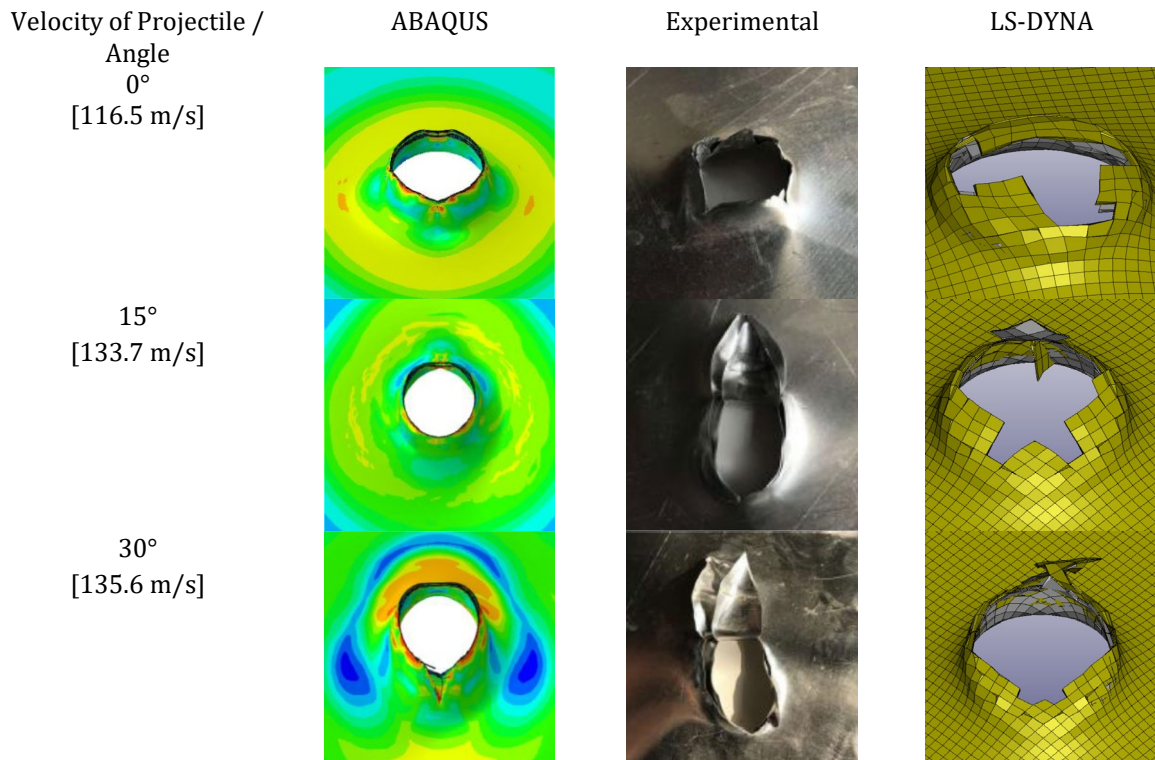


Figure 15. LS-DYNA deformation pattern results for Test 3B, conical nosed projectile impacted against 2 units x 1 mm thickness of circular target plate (double layered target plate) [16]

Table 11. LS-DYNA validation results for Test 4A, hemispherical nosed projectile impacted against 1 unit x 2 mm thickness of circular target plate (single layered target plate) [16]

Angle	Initial Velocity (m/s)	Residual Velocity (m/s)			Percentage Difference (%)	Average Percentage Differences (%)
		ABAQUS	Experimental	LS-DYNA		
0°	131.7	91.8	95.4	94.3	1.2	11.8
	126.0	83.1	89.5	85.6	4.1	
	102.9	21.6	26.5	35.9	30.1	
15°	124.0	82.5	89.9	80.7	10.8	8.1
	117.7	71.3	77.9	69.4	11.5	
	110.6	56.9	61.2	57.0	7.1	
30°	102.5	33.8	39.8	41.0	2.9	45.0
	122.5	64.5	68.6	71.3	3.9	
	111.2	29.8	31.3	54.2	53.6	
	108.5	18.6	21.4	48.4	77.4	

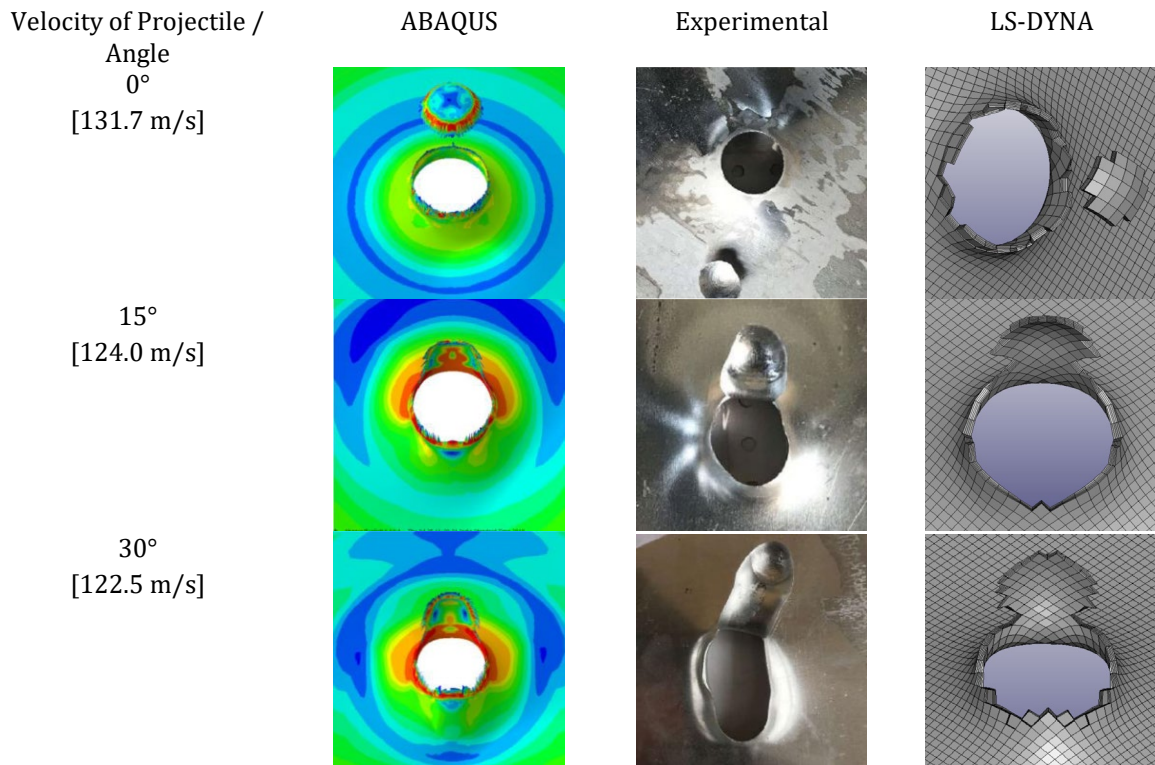


Figure 16. LS-DYNA deformation pattern results for Test 4A, hemispherical nosed projectile impacted against 1 unit x 2 mm thickness of circular target plate (single layered target plate) [16]

Table 12. LS-DYNA validation results for Test 4B, hemispherical nosed projectile impacted against 2 units x 1 mm thickness of circular target plate (double layered target plate) [16]

Angle	Initial Velocity (m/s)	Residual Velocity (m/s)			Percentage Difference (%)	Average Percentage Differences (%)
		ABAQUS	Experimental	LS-DYNA		
0°	122.1	82.6	87.8	92.6	5.3	8.2
	120.1	79.1	83.6	91.4	8.9	
	113.5	68.1	74.5	81.6	9.1	
	105.0	49.2	56.9	62.6	9.5	
	130.4	90.6	95.9	111.0	14.6	
15°	121.2	75.5	73.9	96.2	26.2	32.7
	115.4	64.3	70.8	87.9	21.6	
	102.7	31.5	33.6	68.4	68.2	
	119.2	66.3	70.3	89.8	24.4	
30°	114.2	56.5	61.5	81.5	27.9	38.4
	111.3	48.6	52.3	76.4	37.5	
	105.8	30.5	35.6	68.9	63.7	

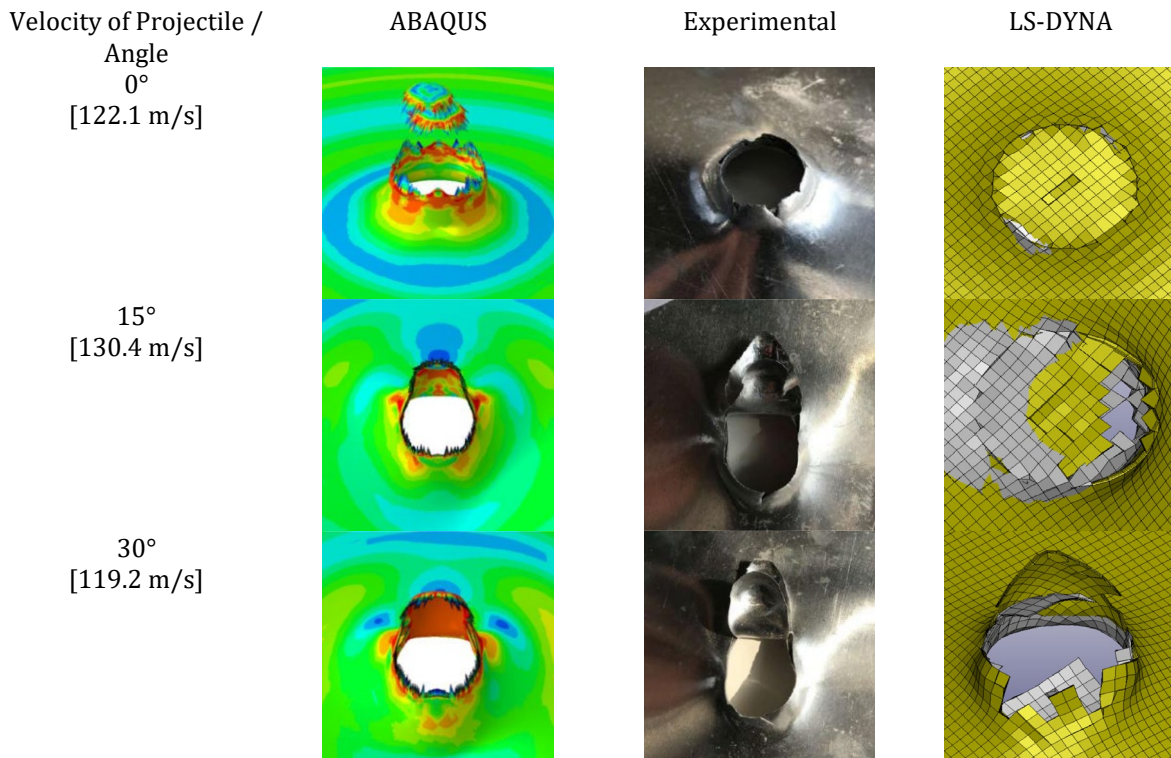


Figure 17. LS-DYNA deformation pattern results for Test 4B, hemispherical nosed projectile impacted against 2 units x 1 mm thickness of circular target plate (double layered target plate) [16]

4.0 CONCLUSIONS

This present study utilizes the numerical simulation analysis i.e. LS-DYNA as a validation tool to predict and compare against previously conducted experimental tests data [16] of the impact performances of four different types of projectiles against single and double layered circular target plate. Eight numerical simulation analyses of four different types of projectiles impacted against single and double layered circular target plate at 0, 15-degree and 30-degrees angle of projectile had been performed. Even though some of the residual velocity average percentage differences predicted by LS-DYNA had large discrepancies with respect to the experimental tests results, an overall residual velocity average percentage differences for all the eight numerical simulation tests results amounted to 16.14 % which can be considered to be a relatively good agreement validation result.

5.0 ACKNOWLEDGEMENT

The authors would like to thank to National Defence University of Malaysia (NDUM) and people who directly and indirectly involve in this writing for their assistance.

List of Reference

- [1] Goldsmith, W. (1999). Non-ideal projectile impact on targets. *International Journal of Impact Engineering*, 22(2-3), 95-395.
- [2] Isiet, M., Mišković, I., & Mišković, S. (2021). Review of peridynamic modelling of material failure and damage due to impact. *International Journal of Impact Engineering*, 147, 103740.
- [3] Koubaa, S., Mars, J., Wali, M., & Dammak, F., "Numerical Study of Anisotropic Behavior of Aluminum Alloy Subjected to Dynamic Perforation," *International Journal of Impact Engineering*, Vol. 101, 2017, 105-114.
- [4] Liu, J., Li, J., Fang, J., Su, Y., & Wu, C. (2022). Ultra-high performance concrete targets against high velocity projectile impact—a-state-of-the-art review. *International Journal of Impact Engineering*, 160, 104080.
- [5] Micallef, K., Sagaseta, J., Ruiz, M. F., & Muttoni, A. (2014). Assessing punching shear failure in reinforced concrete flat slabs subjected to localised impact loading. *International Journal of Impact Engineering*, 71, 17-33.

- [6] Omidvar, M., Iskander, M., & Bless, S. (2014). Response of granular media to rapid penetration. *International Journal of Impact Engineering*, 66, 60-82.
- [7] Signetti, S., & Heine, A. (2022). Transition regime between high-velocity and hypervelocity impact in metals—A review of the relevant phenomena for material modeling in ballistic impact studies. *International Journal of Impact Engineering*, 167, 104213.
- [8] Deng, Y., Wu, H., Zhang, Y., Huang, X., Xiao, X., & Lv, Y. (2022). Experimental and numerical study on the ballistic resistance of 6061-T651 aluminum alloy thin plates struck by different nose shapes of projectiles. *International Journal of Impact Engineering*, 160, 104083.
- [9] Espeseth, V., Børvik, T., & Hopperstad, O. S. (2022). Aluminium plates with geometrical defects subjected to low-velocity impact: Experiments and simulations. *International Journal of Impact Engineering*, 167, 104261.
- [10] Han, J., Shi, Y., Ma, Q., Vershinin, V. V., Chen, X., Xiao, X., & Jia, B. (2022). Experimental and numerical investigation on the ballistic resistance of 2024-T351 aluminum alloy plates with various thicknesses struck by blunt projectiles. *International Journal of Impact Engineering*, 163, 104182.
- [11] Masri, R. (2022). Practical formulae for predicting the ballistic limit velocity of armour perforation by ductile hole growth. *International Journal of Impact Engineering*, 167, 104219.
- [12] Wang, Z. Y., Guo, Q. Q., & Hou, C. C. (2022). Numerical study on the ballistic performance of prestressed concrete slabs subjected to hard missile impact. *International Journal of Impact Engineering*, 168, 104318.
- [13] Xiao, X., Shi, Y., Wang, Y., Chen, X., & Jia, B. (2022). Effect of incorporating Lode angle parameter into a fracture criterion in predicting ballistic impact behavior of double-layered 2024-T351 aluminum alloy plates against blunt projectiles. *International Journal of Impact Engineering*, 160, 104082.
- [14] Ye, S. J., Xu, Y. F., Zhou, Y., Cheng, J. C., Huang, J. Y., Cai, Y., ... & Luo, S. N. (2022). Penetration dynamics of steel spheres into a ballistic gelatin: Experiments, nondimensional analysis, and finite element modeling. *International journal of impact engineering*, 162, 104144.
- [15] Backman, M. E., & Goldsmith, W. (1978). The mechanics of penetration of projectiles into targets. *International Journal of Engineering Science*, 16(1), 1-99.
- [16] Mohammad, Z., Gupta, P. K., & Baqi, A. (2020). Experimental and numerical investigations on the behavior of thin metallic plate targets subjected to ballistic impact. *International Journal of Impact Engineering*, 146, 103717.
- [17] Mohd Nor, M. K., Ho, C. S., Ma'at, N., & Kamarulzaman, M. F. (2020). Modelling shock waves in composite materials using generalised orthotropic pressure. *Continuum mechanics and thermodynamics*, 32, 1217-1229.